PASJ: Publ. Astron. Soc. Japan **63**, 685–696, 2011 June 25

Propagation of Moreton Waves

Yuzong ZHANG,[1,2] Reizaburo KITAI,[1] Noriyuki NARUKAGE,[3] Takuma MATSUMOTO,[1] Satoru UENO,[1]
Kazunari SHIBATA,[1] and Jingxiu WANG[2]
[1]*Kwasan and Hida Observatories, Kyoto University, 17 Ohmine-cho Kita Kazan, Yamashina-ku, Kyoto 607-8471*
yuzong@nao.cas.cn, kitai@kwasan.kyoto-u.ac.jp
[2]*Key Laboratory of Solar Activity, National Astronomical Observatories, Chinese Academy of Sciences, Beijing, China*
[3]*Institute of Space and Astronautical Science, Japan Aerospace Exploration Agency,*
3-1-1 Yoshinodai, Chuo-ku, Sagamihara 252-5210

(Received 2010 August 16; accepted 2011 March 16)

Abstract

With the Flare-Monitoring Telescope (FMT) and Solar Magnetic Activity Research Telescope (SMART) at Hida observatory of Kyoto University, 13 events of Moreton waves were captured at Hα center, Hα $\pm$0.5 Å, and Hα $\pm$0.8 Å wavebands since 1997. With such samples, we have studied the statistical properties of the propagation of Moreton waves. Moreton waves were all restricted in sectorial zones with a mean value of 92°. However, their accompanying EIT waves, observed simultaneously with SOHO/EIT at extreme-ultraviolet wavelength, were very isotropic with a quite extended scope of 193°. The average propagation speeds of the Moreton waves and the corresponding EIT waves were 664 km s^{-1} and 205 km s^{-1}, respectively. Moreton waves propagated either under large-scale close magnetic flux loops, or firstly in the sectorial region where two sets of magnetic loops separated from each other and diverged, and then stopped before the open magnetic flux region. The location swept by Moreton waves had a relatively weak magnetic field as compared to the magnetic fields at their sidewalls. The ratio of the magnetic flux density between the sidewall and the path falls in the range of 1.4 to 3.7 at a height of 0.01 solar radii. Additionally, we roughly estimated the distribution of the fast magnetosonic speed between the propagating path and sidewalls in an event on 1997 November 3, and found a relatively low-fast magnetosonic speed in the path. We also found that the propagating direction of Moreton waves coincided with the direction of filament eruption in a few well-observed events. This favors an interpretation of the "Piston" model, although further studies are necessary for any definitive conclusion.

Key words: shock waves — Sun: chromosphere — Sun: corona — Sun: flares — Sun: magnetic fields

1. Introduction

A Moreton wave, a kind of large-scale shock wave, with an arc-shaped front while propagating in the chromosphere at a speed of 1000 km s^{-1}, was first observed directly by an Hα filtergraph at the Hα line center and wings (Moreton 1960; Moreton & Ramsey 1960; Athay & Moreton 1961; Smith & Harvey 1971).

It has been interpreted that a Moreton wave is a chromoshperic intersection of a flare-produced fast-mode MHD wave propagating in the corona, like a "sweeping skirt" being refracted and bent away from regions of high fast magnetosonic speed and reflected in regions of sharp gradients of the wave speed (Uchida 1968; Uchida et al. 1997). The fast mode MHD shocks in the high corona were thought to be the source of type II radio bursts (Kai 1969). Having experienced a 20-year quiescent phase lacking new, interesting observational cases, the research on Moreton waves, including numerical simulations, has become prosperous again, since a series of stirring coronal disturbances were discovered in multiwavelength observations. What is most important is outstanding globally propagating wavelike disturbances, namely EIT waves observed by the Extreme-ultraviolet Imaging Telescope (EIT: Delaboudinière et al. 1995) aboard the SOHO spacecraft in the low corona in 1997 (Thompson et al. 1998). These waves were considered to be plausible candidates for the coronal manifestation of Moreton waves with some doubt concerning the shape and timing of the wave front, as those observed with EIT were not entirely commensurate with the characteristics of Hα Moreton waves (Thompson et al. 1999). Later, Khan and Aurass (2002) first discovered a soft X-ray disturbance, commonly called "X-ray waves" using the Soft X-ray Telescope (SXT: Tsuneta et al. 1991) aboard the Yohkoh satellite (Ogawara et al. 1991). In He I λ 10830 Å data (hereafter referred to as He I), obtained at the Mauna Loa Solar Observatory, wavelike phenomena were also detected (Gilbert et al. 2004). In addition, radioheliograms in the microwave range (17 GHz) from the Nobeyama radioheliograph (Nakajima et al. 1994) detected coronal wavy disturbances (Warmuth et al. 2004b).

In X-rays, He I and the microwave range (17 GHz), disturbances propagating from the corona to the chromosphere were detected simultaneously with Moreton waves observed in Hα. Moreover, these outstretched observations showing the morphological characteristics and kinematical curves were in accordance with that of Moreton waves. Additionally, the lifetimes were comparable to those of Moreton waves observed in Hα, which were around ten to twenty minutes. Also, the speeds did not contradict that of a MHD fast-mode shock wave (Khan & Aurass 2002; Narukage et al. 2002; Vršnak et al. 2002a;

Warmuth et al. 2003, 2004a, 2004b). However, things are quite different with EIT waves. The arguments about whether the EIT wave is a coronal counterpart to the Moreton wave phenomenon commenced shortly after EIT waves were originally observed. Until now, not enough evidence indicates that the argument has been terminated conclusively.

The following observations are thought to be in favor of the view that EIT waves correspond to fast mode MHD waves. Namely, EIT waves are also associated with soft X-ray flares, and show several characters of waves, such as a decelerating, broadening perturbation profile and a decreasing perturbation amplitude (Thompson et al. 1998; Khan & Aurass 2002; Narukage et al. 2002; Vršnak et al. 2002b; Warmuth et al. 2001, 2003, 2004a, 2004b). This hypothesis was soon attested in model simulations by Wang (2000) and Wu et al. (2001). Using a current-free extrapolation of the measured photospheric field and a density scaling law for coronal loops, Wang (2000) found that the waves are deflected away from active regions and coronal holes where the magnetoacoustic speed is large, and refracted upward to regions where the speed is small. Using a three-dimensional, time-dependent ideal MHD model, Wu et al. (2001) identified "EIT waves" as being fast-mode MHD waves dominated by the acoustic mode.

On the other hand, a notable statistical study (Klassen et al. 2000) has shown that the typical velocities of EIT waves range from 170 to 350 km s^{-1} and reach an average of 271 km s^{-1}; only a third or less of those of Moreton waves range from 330 to $\sim$2000 km s^{-1}. Warmuth et al. (2001, 2004b) and Wu et al. (2001) attributed the large velocity discrepancy to the deceleration of EIT waves and low cadence imaging by EIT. Nevertheless, their argument does not seem to be applicable to the cases where EIT waves propagate without any deceleration (Delannée & Aulanier 1999; Delannée 2000; Zhukov & Auchère 2004). Delannée and Aulanier (1999) found that EIT waves may stop near to the magnetic separatrix; Chen (2009) found that the EIT wave front is cospatial with the coronal mass ejection (CME) frontal loop. Further, EIT waves propagate with broad and almost circular wave fronts, whereas Moreton waves are strongly confined to a narrow sectorial zone with arc-shaped fronts (Eto et al. 2002).

Chen et al. (2002) and Chen, Fang, and Shibata (2005) proposed a model in which the coronal Moreton wave corresponds to a piston-driven shock wave straddling the CME; however, the EIT wave is generated by successive stretching of the coronal field lines during CME eruption, and propagates several times more slowly than a Moreton wave does. This reconciles the discrepancy in velocity between EIT and Moreton waves. Chen's model can also explain the existence of a stationary EIT wave front. In brief, until now the nature of EIT waves has remained elusive (Zhukov & Auchère 2004; Tripathi & Raouafi 2007; Wills-Davey et al. 2007).

As featured above, in contrast to the mostly isotropic propagation of an EIT wave, the propagating region of a Moreton wave is restricted in a much narrower sectorial zone during its whole life. This is an important clue for hinting that there exist different generation mechanisms of an EIT wave and a "Moreton wave". Moreover, what is the real reason that leads to the propagation of a Moreton wave far from isotropy, a "piston" or "blast", or some particular property concerning the coronal magnetized plasma along its propagation path?

In this paper we report our analysis on 13 events of Moreton waves in total, which were observed with the Flare-Monitoring Telescope (FMT: Kurokawa et al. 1995) and the Solar Magnetic Activity Research Telescope (SMART: UeNo et al. 2004) in Hα center, Hα $\pm$0.5 Å, and Hα $\pm$0.8 Å wings at the Hida observatory of Kyoto University. We statistically studied several characteristics of these Moreton waves, their relation to associated phenomena, and the magnetic environment. First, we compared the directions of Moreton-wave propagation to those of the associated filament ejections, provided they were observed. Then, we studied the coronal magnetic field in and around the wave propagation zone, under the assumption of a potential magnetic field with Michelson Doppler Imager (MDI) photospheric magnetogram data. The boundary element method (BEM: Yan & Sakurai 2000; Wang et al. 2002; Eto et al. 2002; Zhang, Y. et al. 2007) was used in deriving the coronal magnetic field. The analyzed magnetic properties include the field strength distribution and the topological features in the corona, i.e., the spatial distribution of the coronal magnetic flux system proposed by Wang and Wang (1996) and Zhang, Y. et al. (2007). Finally by taking the event on 1997 November 3 as an example, we derived and analyzed the coronal 3D distribution of the fast-mode MHD wave speed. A few different coronal mass density models were assumed in our study. We believe that our study will be a new attempt to estimate the coronal MHD wave speed distribution, based on the observed data.

The next section gives a description of the observations and data analysis. Section 3 is a summary of the main results in this study. Section 4 is devoted to a discussion on the implications of these results. Our conclusion is given in section 5.

2. Observations and Data Analysis

2.1. *Data Source*

Two solar Hα telescopes, FMT and SMART at Hida observatory of Kyoto University, captured a total of 13 events of Moreton waves (see table 1) since 1996. The FMT observes five full-disk images in Hα center, Hα $\pm$0.8 Å, and white light, and one solar-limb image in Hα center simultaneously with a cadence of one minute and a spatial resolution of around 4″. Besides the three Hα wavelengths mentioned above, SMART observes in two other Hα wing images, i.e., Hα $\pm$0.5 Å with a normal cadence of two minutes and a spatial resolution of 0.″5. The FMT detected the former 10 events, while the SMART captured the later three events associated with three consecutive homologous M-class X-ray flares in its five wavebands at Hα center, $\pm$0.5 Å, and $\pm$0.8 Å (Narukage et al. 2008). An extensively explored event, which occurred on 1997 November 3 (Warmuth et al. 2001, 2002; Khan & Aurass 2002), was described at length as an example for us in accounting for the use of data, and the method in this work. From observations of SOHO/EIT, we checked the corresponding EIT waves if they existed (see table 1).

2.2. *Tracking the Wavefronts of Moreton Waves*

At 04:32 UT on 1997 November 3 an X-ray C8.6 class flare occurred in the active region AR 8100, which was recorded by

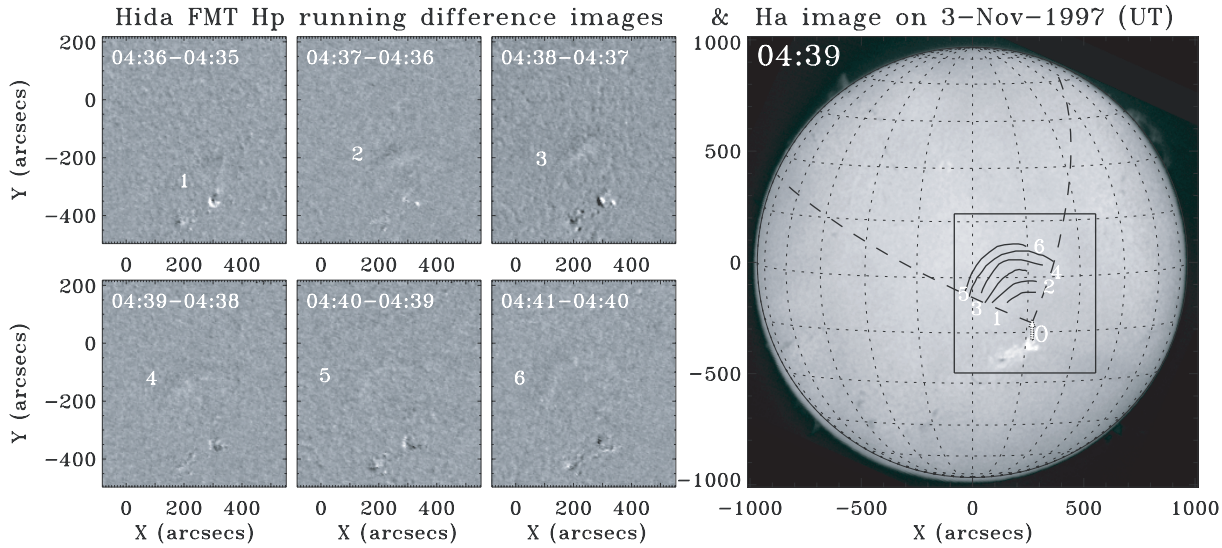

Fig. 1. H-alpha images observed with Hida FMT in Hα line center and Hα line wing (+0.8 Å) (Hp) on 1997 November 3. The six left panels are the running difference images in Hp and the Moreton-wave fronts shown with the Arabic numbers from "1" to "6". The right panel is a solar image in the Hα line center. The circle and the rectangle in black in the right panel show the solar limb and the field of view of six other sliced images. The dashed black lines show the edge of the track of Moreton wave. The six solid black curves are the six Moreton-wave fronts in the six sliced images. The dashed open arrow in the right panel denotes the direction of filament eruption.

Geostationary Operational Environmental Satellites (GOES). Three minutes later, with the observations in Hα line center, and red and blue wings, FMT captured a Moreton wave that was visible from 04:36 UT to 04:41 UT. Two rows of panels in the left part of figure 1 are six running difference images (Thompson 1998; Sheeley et al. 2004) in Hα +0.8 Å, where we can clearly see the propagation of the wave front. The location of the front at each instant is indicated by Arabic numbers, "1" to "6". To display the propagation process of the Moreton wave conveniently, we overlay the wavefront locations in black solid lines on the full-disk image in the Hα line center in the right panel of figure 1. The black square denotes the same field of view shown in the six left panels. Letter "O" marks the eruption position, and Arabic numbers "1" to "6" are similar to those in the six left panels. The span angle of the wave in its propagating process could be measured by two intersecting black dashed lines, which indicate the two edges of the propagation sector. By running difference images taken in the Hα and EUV wavebands, we identified the wavefronts of the Moreton waves and EIT waves in 12 other events. Following the style of figure 1 in Warmuth et al. (2004a), analogously, figure 2 shows the locations of the fronts of the Moreton wave in black and the EIT wave in gray of 12 other cases overlayed on Hα filtergrams. Generally, the lifetime of the Moreton waves is less than 10 min. For the much lower temporal cadence ($\sim$ 12 min) of EIT observations, fewer wavefronts of the EIT wave, e.g., three wavefronts at most, were detected. We could not confirm the accompanying EIT waves for two cases in the 12 Moreton-wave events. One of the two was due to the SOHO data gap on 1998 August 8. Therefore, the association of Moreton waves and EIT waves seems to be highly probable. On 2000 June 15 and 2004 November 3, the EIT waves were "split" and propagated in almost oppositive directions.

By using movies made based on those images obtained at the Hα center and wing wavebands, we compared the directions of the propagating of Moreton waves and those of accompanying filament eruptions. In figures 1 and 2, those dashed open arrows show the directions of eruption filaments. The directions of filament eruptions were generally the same as those of the Moreton wave propagations.

Table 1 exhibits an overview of these 13 events of Moreton waves with 10 columns. The first column is the dates of the 13 events with event codes by "E" and the serial number. The active region numbers, their locations, and the importances of associated flares are listed in the three following columns. Then, three columns of time information follow: the beginning and peak times of the associated flares, the times of CME in the corresponding temporal windows observed first by LASCO/C2, and the start times of Moreton waves. The 8th and 9th columns give the wave-front-detected frame numbers in the Hα observations of FMT or SMART and in the EUV 195 Å observations by EIT, respectively. The last column lists literature where the same events were studied by other researchers.

2.3. Extrapolating Photospheric Magnetic Field to Corona

To explore the role of the coronal magnetic field in the process of Moreton wave propagation, we reconstructed the global coronal magnetic field based on the potential field assumption.

Figure 3 shows the 3D magnetic lines of force from the extrapolated coronal magnetic field on 1997 November 3 and 2001 May 12, by using the method of BEM (Yan & Sakurai 2000) with the composite synoptic magnetogram, whose central longitude zone ($\pm$60°) and latitude zone ($\pm$80°) are replaced by the MDI full-disk magnetogram (Zhao et al. 1997; Wang et al. 2002; Zhang, Y. et al. 2007). The green, yellow, and red lines represent the magnetic field line with the maximum heights < 0.3, 0.3–1.0, and > 1.0 solar radii,

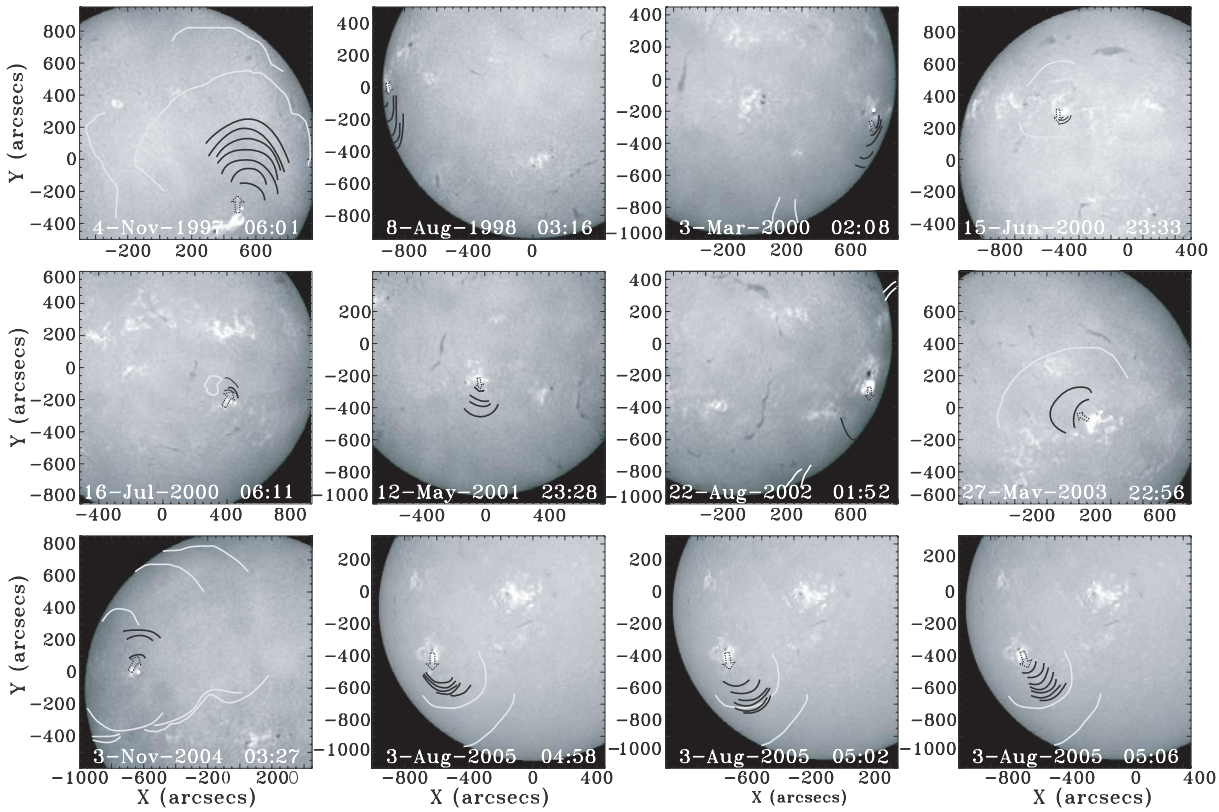

Fig. 2. Twelve other events of Moreton wave: those black and gray lines show the wavefronts of Moreton waves and EIT waves superposed on Hα filtergrams which refer to the work from Eto et al. (2002) and the Narukage's webpage.[1] In these images, solar north is up, west is right, and time is given in UT. Dashed open arrows denote the directions of filament eruptions in each panel.

respectively. The white square in the left panels denotes the field of view of the right panels. The backgrounds in the left and right panels are, respectively, MDI full-disk magnetograms and FMT Hα filtergrams at the red wing.

To study the spatial distribution of the extrapolated coronal magnetic field strength in the propagating area of the Moreton wave and EIT waves, we took a three-step approach to extract the common features in eight events that took place not far from the disk center. In the first step, we introduced a spherical coordinate system. The pole point, which is marked with a capital letter "O" in figure 4, was taken to be the center of curvature of the initial Moreton wave front. Next, we put the central propagating direction of the Moreton wave along the longitude 180° of the sphere indicated by a black arrow. The area swept by the Moreton wave is emphasized by thick darker gray grids. If there was a corresponding EIT wave, the propagation zone of the EIT wave will be overlayed in brighter gray. On 1997 November 3, the span angles of the Moreton wave and EIT wave were 87° and 145°, respectively. The central directions of these two waves were virtually the same. However, in other cases, two central lines were separated. What is more, on 2001 May 12, 2002 August 22, and 2004 November 3, the wavefronts of the EIT waves even were split into two branches with quite different orientation. Finally, we divided the sphere (see figure 4) by 10 concentric circles with a step of 0.1 solar radii of the Sun and 24 meridian lines with an interval of 15°. In such a way, the meridian lines are used to denote the propagation direction of the Moreton waves. Figure 5 and figure 6 represent the distributions of the mean coronal magnetic strength at the heights of 0.01 solar radii on 10 concentric circles in sequence shown in figure 4. The angular extents swept by the Moreton waves and related EIT waves (if they exist) are indicated in a black grid and in bright gray, respectively. One thick black line and nine thin black lines denote the mean magnetic field strengths of the innermost circle and nine outer ones in order, respectively.

3. Results

3.1. Comparison between the Propagations of Moreton Waves and EIT Waves

In table 2 we summarize the dynamic properties of the 13 cases of Moreton waves and EIT waves if the relevant EIT observations are available. The maximum, minimum, and average span angles of the Moreton waves were, respectively, 136°, 45°, and 92°, which were all much smaller than those of the corresponding EIT waves, i.e., 360°, 140°, and 193°, respectively. The difference in the span angle of propagation between the Moreton waves and EIT waves was clearly confirmed in this work. It seems to be important to explain these characteristics in theoretical modelings.

The mean velocity of EIT waves, 205 km s^{-1}, was found to be just one third of Moreton waves, 664 km s^{-1}. The acceleration of the Moreton wave was quite small. The accelerations

[1] ⟨http://www.kwasan.kyoto-u.ac.jp/~naru/studies/index.html⟩.

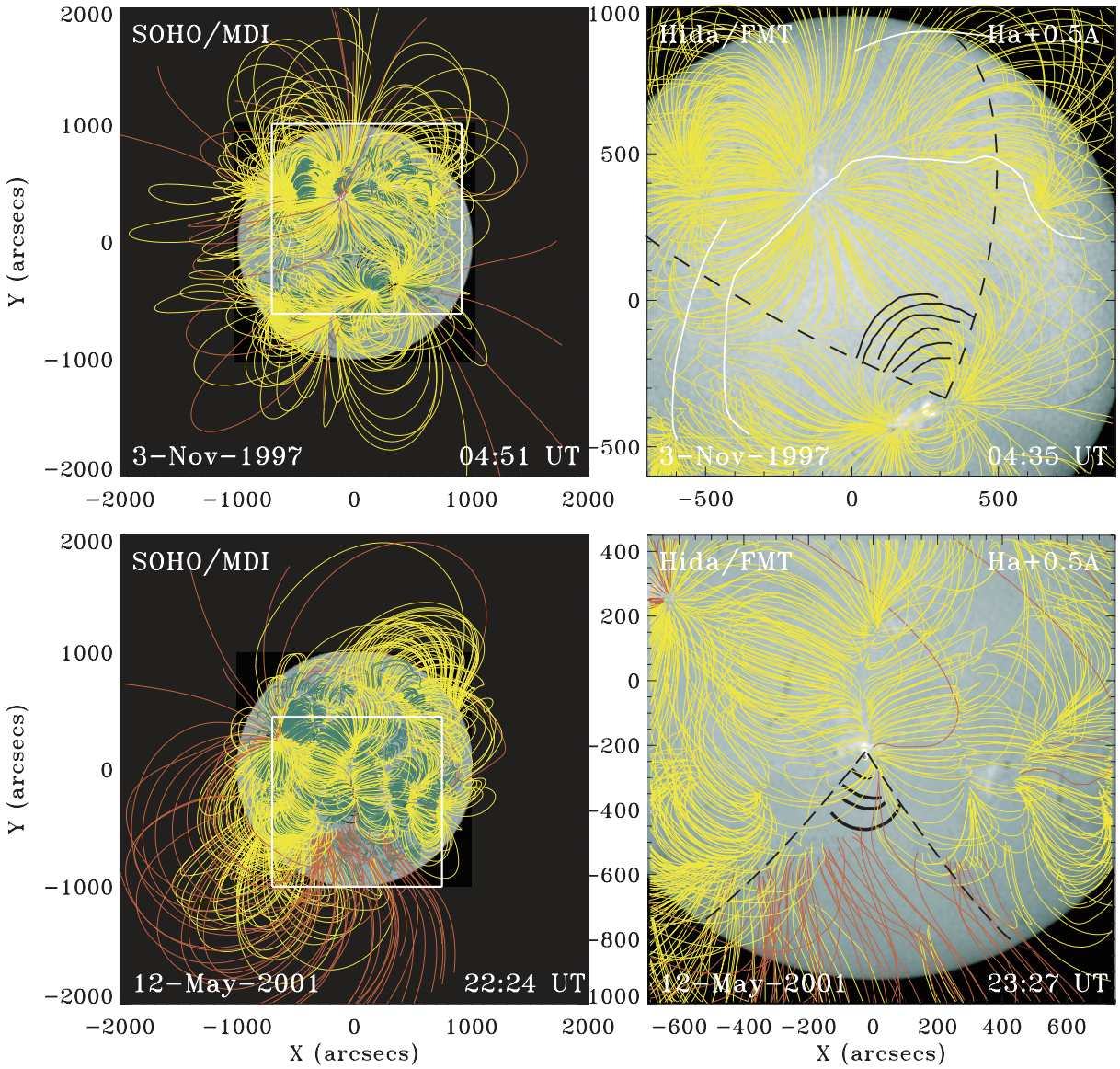

Fig. 3. Two types of magnetic connectivity of Moreton-wave propagations, in which their wavefronts are shown in black lines on the left column referring to the Narukage's webpage:[1] one is under a large-scale closed magnetic loop and the other along the path where two sets of magnetic loops diverge. The left panel represents the total extrapolated magnetic field superposed on MDI daily magnetograms on 1997 November 3 (upper) and 2001 May 12 (lower); the right one zoom in on the field of view denoted by white square in the left panel with the background of Hα filtergram. The green, yellow, and red lines represent the three magnetic field lines of which heights are lower than 0.3, from 0.3 to 1.0, and higher than 1.0 solar radii of the Sun, respectively.

of EIT wave propagations are actually difficult to measure with the 12 min cadence observations of SOHO/EIT. Among the 13 events of Moreton waves, only in case E10 were three EIT images in 195 Å obtained, and its acceleration was measured to be 0.03 km s^{-2}, which is also quite small.

Additionally, unlike EIT waves, the directions of the propagation of Moreton waves matched those of accompanied filament eruptions quite well.

3.2. *Magnetic Topology of the 3D Extrapolated Coronal Magnetic Field*

By a comparison of the propagating paths of Moreton waves to the structures of the coronal magnetic field, we found that the Moreton wave on 1997 November 3, shown in the upper panels in figure 3, propagated under a set of trans-equatorial loops connecting AR 8100 with AR 8102. In another case of a Moreton wave on 2001 May 12 in the lower panels, we identified that the wave propagated in the sectorial region where two sets of magnetic loops separated from each other and diverged, without entering the south-pole area of a dominantly open flux. We studied the magnetic connectivity and the wave propagating paths for all events, except for the limb ones, such as those on 1998 August 8, 2000 March 3, and 2005 August 3. It was found that the Moreton waves on 1997 November 4, 2000 June 15, 2000 July 16, and 2003 May 27 propagated similarly under large-scale closed magnetic loops; however, others, e.g., those on 2002 August 22 and 2004 November 3, propagated toward open magnetic flux in a similar magnetic environment

Table 1. Overview and data coverage of 13 Moreton-wave events observed with FMT and SMART at Hida observatory of Kyoto University.*

Event	NOAA No.	Flare loc.	Flare imp.	SXR beg.–max.	CME (C2)	1st Moreton	n Ha	n EIT	References
E1: 1997 Nov 3	8100	S20W13	SB/C8.6	04:32–04:38	05:28	04:36	6	2	Warmuth et al. (2004a, 2004b)
E2: 1997 Nov 4	8100	S14W33	2B/X2.1	05:52–05:58	06:10	05:58	7	2	Eto et al. (2002)
									Narukage et al. (2002)
									Warmuth et al. (2004a, 2004b)
E3: 1998 Aug 8	8299	N13E74	1B/M3.0	03:12–03:17	–	03:17	5	–	Warmuth et al. (2004a, 2004b)
E4: 2000 Mar 3	8882	S15W60	1B/M3.8	02:08–02:14	02:30	02:12	5	2	Narukage et al. (2004)
									Warmuth et al. (2004a, 2004b)
E5: 2000 Jun 15	9040	N19E19	1F/M2.0	23:36–23:43	24:26	23:39	2	1	
E6: 2000 Jul 16	9082	S08W25	1N/C3.8	06:08–06:14	06:54	06:10	3	1	
E7: 2001 May 12	9455	S17E00	1B/M3.0	22:42–23:35	23:00	23:28	4	–	
E8: 2002 Aug 22	10069	S07W62	2B/M5.4	01:47–01:57	02:06	01:59	1	2	
E9: 2003 May 27	10365	S07W17	2B/X1.3	22:56–23:07	23:50	23:03	2	1	
E10: 2004 Nov 3	10696	N08E45	1M/M1.6	03:23–03:35	03:54	03:28	1	4	
E11: 2005 Aug 3	10794	S13E45	M3.4	04:54–05:06	05:30	04:59	5	2	Narukage et al. (2008)
E12:						05:01	6		
E13:						05:04	7		

* "Event" gives the event label and date; "NOAA No." the active region number; "Flare loc." the coordinates of the flare; "Flare imp." the optical and soft X-ray importance of the flare; "SXR beg.-max." the times of beginning and maximum of the SXR flare; "1st Moreton" the time of the first Moreton wavefront; and "n" the number of identified wavefronts in the various spectral bands. "–" means that no wave feature could be detected, and a blank space indicates that the information is the same as the above. Literature related with the same event is listed in the last column.

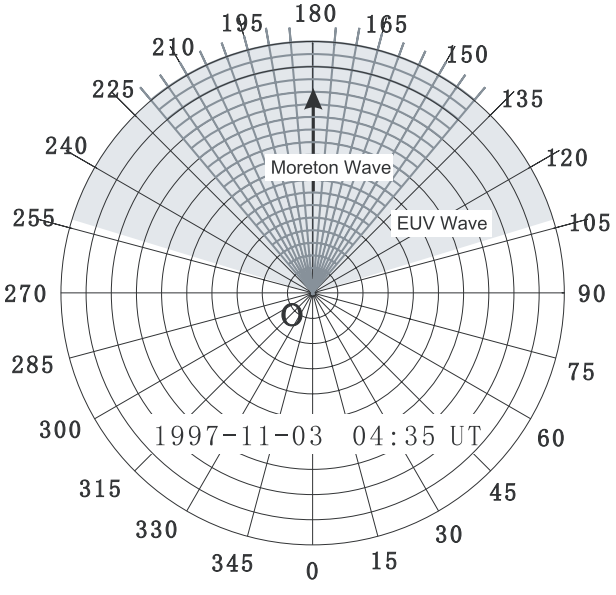

Fig. 4. Sketch denoting the region swept by a Moreton wave (darker gray grids) and an EIT wave (brighter gray background) on 1997 November 3. The black arrow marks the central direction of the Moreton wave on 180°. The letter "O" marks the wave initiation point.

Table 2. Dynamic properties of these 13 Moreton waves and relevant EIT waves.

Event	Span angle		Velocity		Acceleration	
	MW	EW	MW	EW	MW	EW
E1	87	145	539	315	0.5	–
E2	126	175	734	80	−0.4	–
E3	136	–	845	–	−3.6	–
E4	87	150	826	159	1.8	–
E5	97	144	294	–	–	–
E6	45	360	330	–	5.1	–
E7	70	–	646	–	0.2	–
E8	92	161	–	129	–	–
E9	94	141	1490		–	
E10	80	318	1043	279	−19.2	0.03
E11	107	140	324	269	−0.8	–
E12	83	–	476	–	−1.9	–
E13	91	–	426	–	−0.9	–
Mean	92	193	664	205	−1.9	0.03
σ	23	84	352	95	6.5	–

* Moreton wave and EIT wave are abbreviated as "MW" and "EW" here; the units of span angle, velocity, and acceleration are degrees, $km\,s^{-1}$, and $km\,s^{-2}$ respectively. The last two lines are the average value and standard deviation.

to that for the event on 2001 May 12. Therefore, Moreton waves propagate in regions of simple magnetic morphologies, either under large-scale magnetic loops, or under diverging loop systems but will stop before those open magnetic flux.

This simple magnetic morphology favorable to Moreton wave propagation suggests to us that the magnetic field strength will be relatively small in these regions. We will discuss this relationship in the next subsection.

3.3. Moreton Wave Propagation and Coronal Magnetic Field Strength

Regardless of the magnetic topology of the wave propagating region, either under a closed magnetic loop or diverging loop systems, Moreton waves are "flowing" in the "valley"

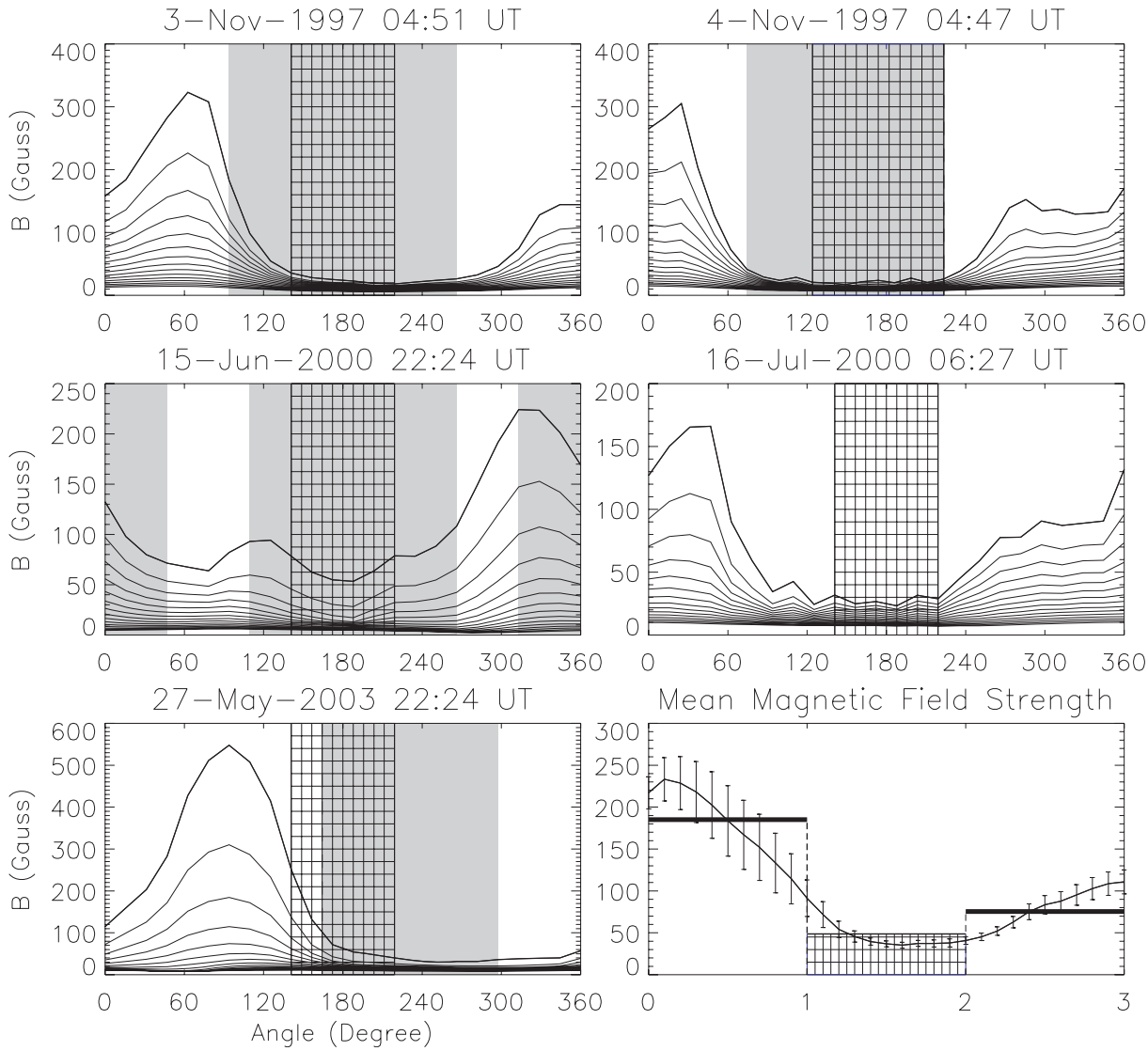

Fig. 5. Ambient magnetic field distributions in the five events of Moreton waves that propagated under a large-scale magnetic loop. In the first five panels, the black grid and bright gray background show the regions swept by the Moreton wave and the EIT wave, respectively. The distributions of the mean coronal magnetic strength at the height of 0.01 solar radii and around the ignition points by 10 concentric circles shown in figure 4 are plotted by black curve lines. One thick and nine other black lines denote the innermost circle and the nine outer layers in order. The lower-right panel represents the normalized magnetic fields in the region swept by the Moreton wave as well as its left and right regions with the equivalent area. They are 50, 185, and 75 gauss on average.

being made of a stronger magnetic field on both of their sides. In the bottom-right panel of figure 5, the mean flux densities of the 5 events on the path and the left and right walls normalized with the equal area are shown to be 50, 185 and 75 gauss, respectively. Similar average values for the remaining 3 events are shown to be 122, 170, and 215 gauss, respectively, in figure 6. In other words, Moreton waves, indeed, tend to propagate along paths in weak magnetic regions, and to be confined to those stronger magnetic regions, like "walls" (Uchida 1968). Unlike Moreton waves, there were no close relations between the path of EIT wave and its ambient magnetic field. It was first demonstrated observationally and statistically that the paths of Moreton waves are clearly characterized by weaker coronal magnetic fields.

4. Discussion

Let us discuss the propagation of the coronal counterparts of Moreton waves. The fast-mode magnetoacoustic speed near the solar surface is lower than that in the low corona. Therefore, the normal direction of the fast-mode wave fronts in the low corona would point to the solar surface, which makes it easier for the wave to compress the chromosphere. To see the coronal distribution of fast magnetoacoustic speed, which is determined by the local plasma density and magnetic field, we tried three rough estimates for the event on 1997 November 3, by adopting three different methods for calculating the coronal density, with the same potential coronal magnetic field calculated by the method described above. To simplify the calculation, as indicated in panel A of figure 7, only seven cross

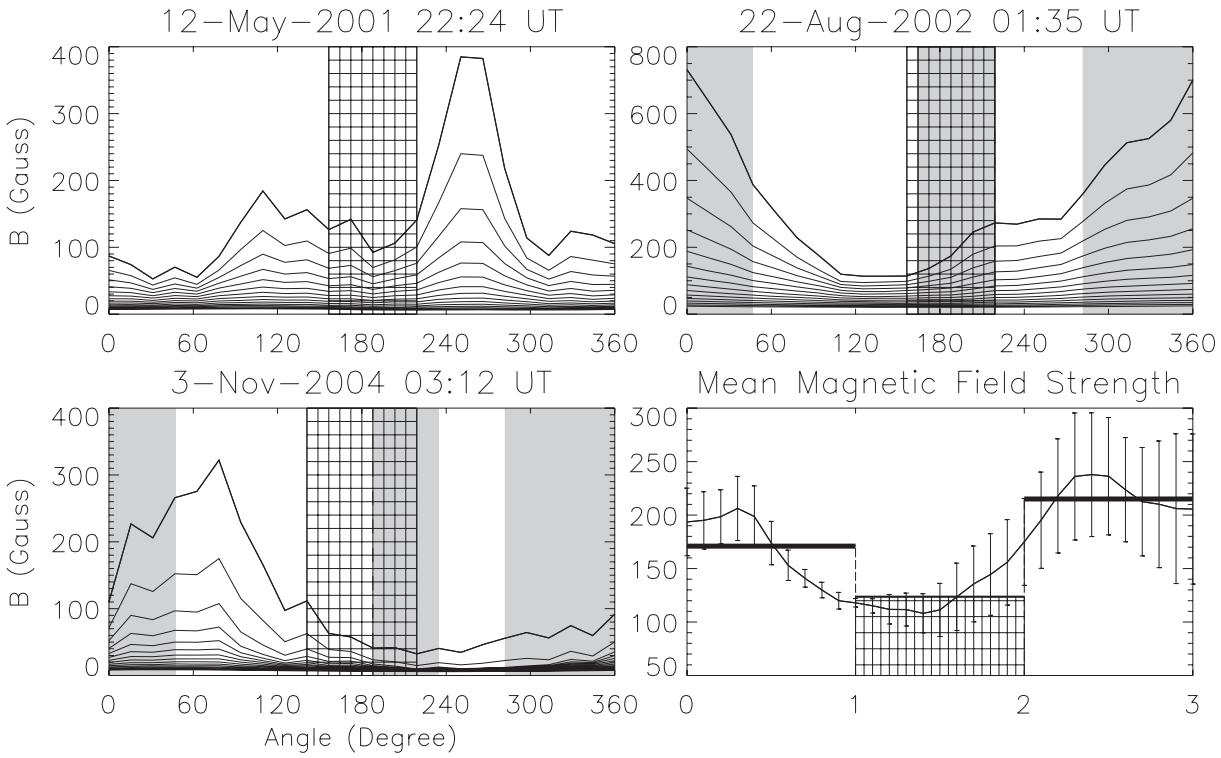

Fig. 6. Ambient magnetic field distributions of the three events of Moreton waves, propagating to those areas of dominant open flux. In the first three panels, the black grid and bright gray background show the regions swept by the Moreton wave and the EIT wave, respectively. The distributions of the mean coronal magnetic strength at the height of 0.01 solar radii and around the ignition points by 10 concentric circles shown in figure 4 are plotted by black curve lines. One thick and nine other black lines denote the innermost circle and the nine outer layers in order. The lower-right panel represents the normalized magnetic fields in the region swept by Moreton wave as well as its left and right regions with the equivalent area. They are 122, 170, and 215 gauss on average.

sections extending over seven directions, marked with Arabic numbers "1" to "7", were studied. Among them, directions of "3", "4" and "5" lie in the propagating path of the Moreton waves; "2" and "6" are exactly on the two borders, while "1" and "7" are slightly out of the propagation zone.

In the first method (hereafter referred to as M1), we assumed that the force balance was maintained between the pressure gradient and the gravitational force, without any contribution from the Lorentz force (Priest, 1982). The temperature distribution over the solar surface was derived by the ratio of 195 Å to 171 Å intensities obtained from the SOHO/EIT observations (Benevolenskaya et al. 2001; Zhang, J. et al. 2007). It may increase with height (Aschwanden & Acton 2001). However, to simplify the calculation of deriving the 3D coronal density distribution, we assumed a constant-temperature corona in the radial direction and a uniform distribution of the density at the bottom with a value of $1.0 \times 10^9\,\mathrm{cm}^{-3}$. Thus, method M1 is a very crude one, but we believe that it is useful to see the large-scale spatial distribution of the fast magnetoacoustic speed. The calculated fast magnetoacoustic speed distributions in seven cross sections are shown in panels B to H in figure 7. Panels C to H have the same size of the field of view as a fan-shaped region delineated with red lines in panel B with the height of 0.8 solar radii and a span angle of 1.2 radian. Point "O" represents the initial site of Moreton waves, and the red arrows indicate the same directions as those of seven red arrow lines in panel A. The brighter (darker) blue means higher (lower) fast magnetoacoustic speed, with their contours being overlayed. The highlight contour in yellow represents the value of the fast magnetoacoustic speed of $400\,\mathrm{km\,s}^{-1}$. In lines "3" to "7", especially line "4", a low-velocity domain of fast-MHD wave is present at the low corona in the quiet region between the two active regions. If a wave ray is emitted with a high inclination from the vertical, i.e., nearly horizontal ray of the wave, it will be bent down to the surface, and will be observed as the front of a Moreton wave. On the other hand, the rays emitted with low inclinations will propagate to higher corona without impinging to the chromosphere. About those rays emitted with medium inclinations, they will be slightly deflected to lower heights in the corona above the quiet region, but will be deflected to the higher corona again due to the presence of another active region in the course of their propagation. Thus, the decay or disappearance of a Moreton wave front along the propagation will depend on the 3D distribution of the fast-MHD velocity in the corona, and also on the directional distribution of wave power emission.

As is generally well known, different coronal structures such as the active region, the quiet region, the coronal hole, and the coronal streamer have different density distributions in the corona. Consequently, in the two following estimates (hereafter referred to as M2 and M3), different density models in these regions and their changes with the heights are

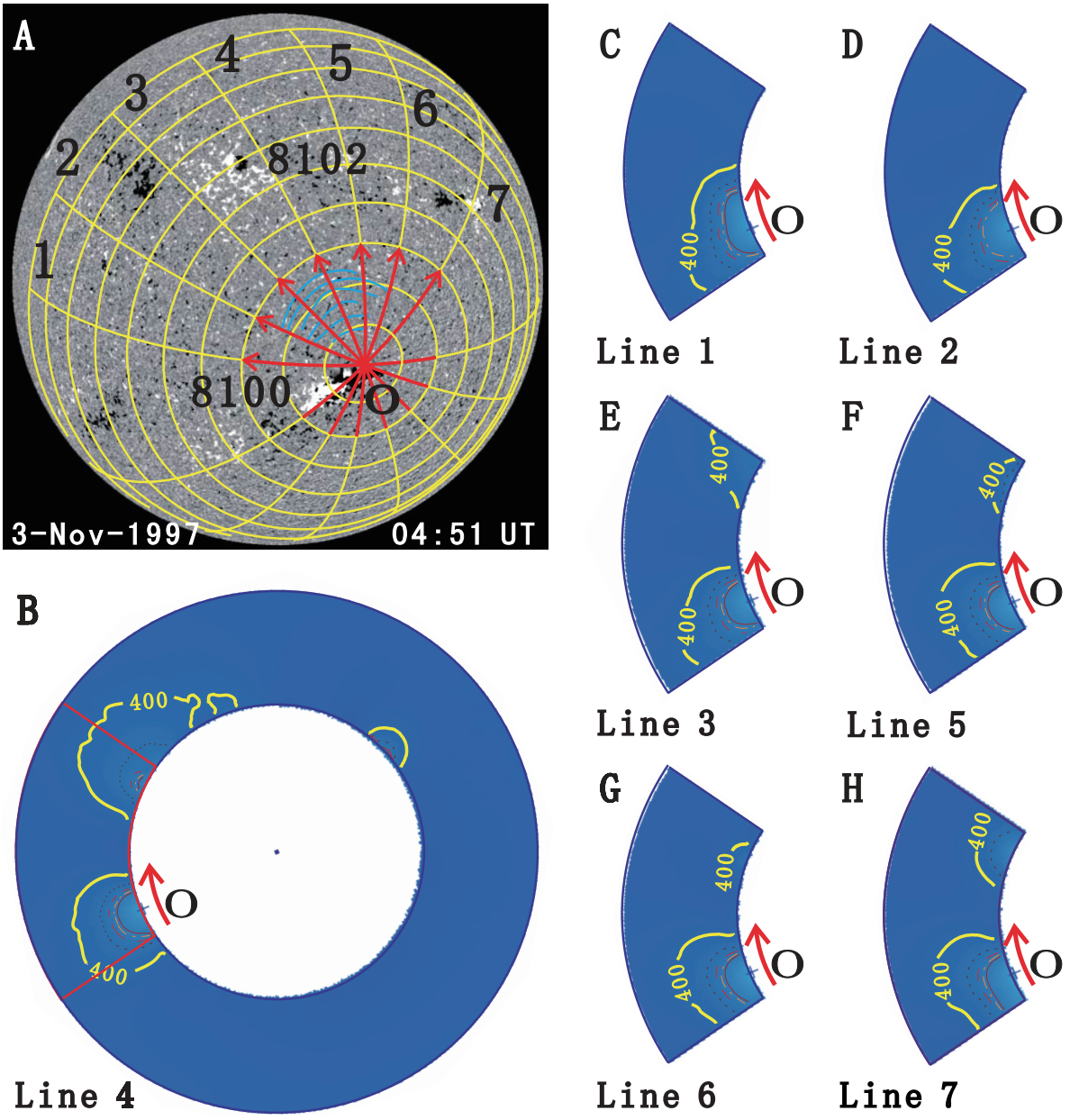

Fig. 7. Moreton wave on 1997 November 3 and maps of calculated fast magnetoacoustic speed distributions by M1 in the seven directions. In panel A, six blue lines denote the wave fronts of the Moreton wave superposed on the MDI daily magnetogrmas at 04:51 UT; seven red lines with arrows marked by Arabic numbers "1" to "7" indicate seven directions with the length of 0.6 solar radii. Among these lines, line "4" is just located in the central direction during the propagation of Moreton waves, and line "2" and line "6" lie on the left and right borders of their propagating scope; "O" means the original point of the wave. Panel B shows the map of the distribution of Alfvén speed in a vertical plane passing through line "4" with the height of 0.8 solar radii. Panels C to H have the same view of field as the red fan-shaped region denoted in panel B with the distance between the −0.2 and 1 solar radii from the original point. Brighter and darker blue mean higher- and lower-fast magnetoacoustic speeds, respectively. Red arrow lines denote the propagating directions. Yellow contour lines mean a speed of 400 km s^{-1}; four other contour levels marked by a different line and color are 800, 1200, 1600, and 2000 km s^{-1}, respectively.

taken in accordance with the magnetically different regions, as mentioned above (Aschwanden & Acton 2001). In the same way as M1, we acquired the temperature over the solar surface and in the corona. The plasma in three models is not in the force equilibrium.

In M2, we discriminated two types of magnetic regions, which were active regions and quiet regions, within and close to the propagating zone of the Moreton wave, in MDI daily photospheric magnetograms. To avoid artificial large-density gradients on the borders between the active region and the quiet Sun, we assumed a Gaussian density distribution so as to acquire a continuous distribution from the center of the active region to its border. In figure 8, the first two rows of panels, marked by "A", give maps of the distribution of the fast magnetoacoustic speed calculated by M2 in the same seven vertical planes as mentioned above. It was found that a "valley"

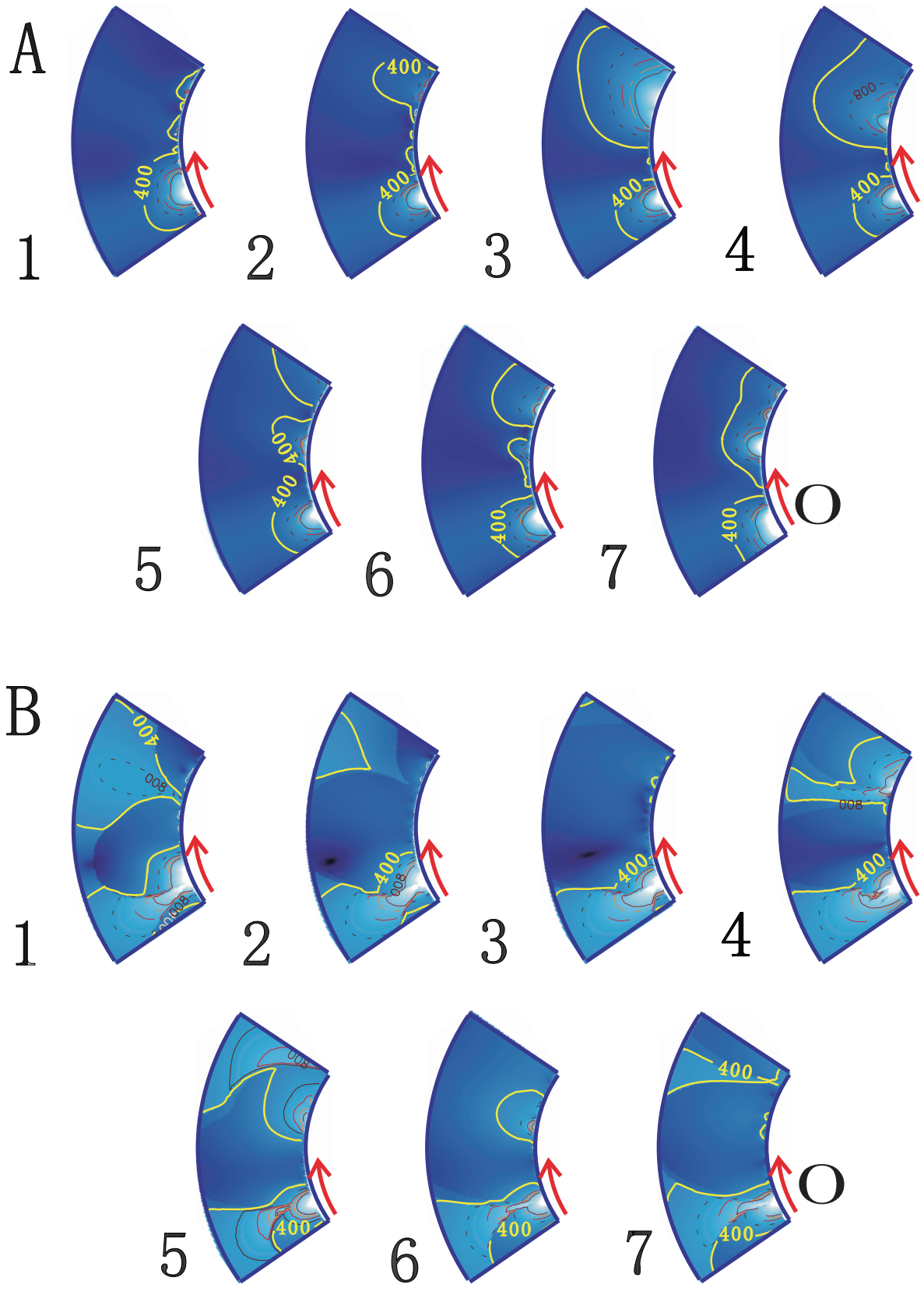

Fig. 8. Maps of the calculated fast magnetoacoustic speed distributions by M2 (the two upper rows) and M3 (the two lower rows) in the same regions as those in figure 7. Similarly, "O" means the original point of the wave, red arrow lines the propagating direction and the distance, and yellow contour lines a speed of 400 km s^{-1}; four other contour levels are 800, 1200, 1600, and 2000 km s^{-1}, respectively.

gradually forms from the first cross section to the third one, which shows the most remarkable "valley", and then is filled to disappear slowly.

During the previous two methods, the density is monotonously decreasing along the radial direction. However, dominated by complicated connectivity of coronal magnetic field, the actual density distribution of coronal plasma is extremely complex and far from a monotonous variation almost along any radial directions. In brief, the connectivity of the coronal magnetic field should not be ignored. We will take account of this effect in M3. Here, according to the height and the distance between two footpoints, we discriminated three types of coronal magnetic loops. If the height of a flux loop was higher than 1.5 solar radii, the flux loop was identified as being an "open flux loop". Similarly, if the height of a flux loop was higher than 0.6 solar radii and lower than 1.5 solar radii, or its height is greater than its distance between two footpoints, then the flux loop was treated as a "coronal streamer". The others were "active region loops". The values at the base of three types of the flux loops, i.e., "open flux loop", "coronal streamer" and "active region loop", are $\sim 1.0 \times 10^8$, 2.0×10^8, and $5.0 \times 10^8\,\mathrm{cm}^{-3}$, respectively. Hence, referring to the density model from Aschwanden and Acton (2001), we could obtain the density of a given point by the type of magnetic loop passing it and its height. In figure 8, the last two rows of the panels, marked by "B", exhibit the result of M3. We can see that the same characteristics as those of M1 and M2 hold in M3; i.e., between the active regions 8100 and 8102, the fast magnetoacoustic speed is relatively low. Summing up the results of our estimates to obtain the fast magnetoacoustic wave speed distribution in the corona, we found that there is a channel with a relatively low-fast magnetoacoustic speed in the zone of the Moreton wave propagation, irrespective of the coronal density models assumed.

This means that the Moreton wave propagates along a channel of low fast magnetosonic speed. The characteristics are consistent with both the "blast wave" theory and the "piston wave" theory. In the "blast wave" theory, the energy explosively deposited in the flare site flows out along the low magnetosonic speed channel as a Moreton wave. Filament ejection will also be forced to go through the weak magnetic field channel guided by the surrounding strong magnetic field; or the filament ejection, itself, may be driven by the passage of a shock wave, which eventually propagates as a Moreton wave. On the other hand, in "piston wave" theory, the filament ejection direction and the Moreton wave direction will be guided in a similar way to the "blast wave" theory case, by the surrounding global coronal magnetic field configuration. Thus, we cannot easily tell which theory is applicable to the phenomenon of a Moreton wave, judging from our present work. A detailed study of the temporal evolution of filament ejection and the emission of a Moreton wave at the flare site will be necessary for a decisive conclusion.

5. Conclusion

During the period between 1997 and 2005, 13 events of Moreton waves were observed in the Hα center and wings at Hida observatory of Kyoto University.

By tracking their propagations, we found that the mean span angle of Moreton-wave propagation was 92°, which was approximately half of the mean span angle for the corresponding EIT wave. This indicates that the propagation of a Moreton wave is far from isotropic. Meanwhile, the average velocity of Moreton waves was $660\,\mathrm{km\,s}^{-1}$, which was higher than that of EIT waves by a factor of three, which is consistent with earlier determinations.

Considering the key role of the magnetic field in solar activities, we estimated the 3D coronal magnetic field based on SOHO/MDI line-of-sight magnetograms in the photosphere by the extrapolation of those Moreton-wave events that took place not far from the disk center, and compared their connectivity and flux density with the propagation of Moreton waves in these events.

Firstly, a comparison between the coronal magnetic connectivity and the Moreton-wave propagation suggests two associated connectivity patterns: Moreton waves propagate either under large-scale closed magnetic loops or in the region where two sets of coronal loops separate from each other and diverge. In the latter case, the waves propagate toward the open magnetic flux, but without entering it.

Secondly, the coronal magnetic field along the path of Moreton waves was relatively weak, while the magnetic field on both sides of the path was stronger, whatever type of connectivity patterns it relates to. The ratio of the coronal magnetic flux density between both sides and the path is in the range of 1.38 to 3.70 at a height of 0.01 solar radii. A relatively weak magnetic channel with its stronger ambient magnetic fields forms a magnetic "valley", where a Moreton wave propagates, and filament ejection is also compelled to pass through.

Therefore, the coincidence of the propagation direction of a Moreton wave and the magnetic "valley" presents two probable explanations: one follows the "piston" model (Chen et al. 2002); the other is that the "blast" wave is refracted by "magnetic walls" of the "valley" (Uchida 1968; Steinolfson et al. 1978). At present, we cannot tell which model, the "piston" or "blast wave", is a plausible mechanism of Moreton-wave initiation. Nevertheless, we think that the newly revealed magnetic connectivity patterns and a relatively weaker magnetic field of the wave propagation path shed new light on understanding the true physics of these models.

Additionally, by comparing the propagation of a Moreton wave with that of an EIT wave, we find that EIT waves could propagate through a stronger magnetic field regime in the vicinity of the originating active region; on the contrary, Moreton waves always avoid these stronger magnetic regions. This seems to mean that an EIT wave does not belong to the regime of fast-mode magnetoacoustic waves. Chen et al. (2002) proposed that the propagation of an EIT-wave front comes from successive stretching of all field lines. Wang, Shen, and Lin (2009) suggested that an EIT wave is a kind of slow-mode shock wave that will decay somewhere in the lower corona before arriving at the bottom boundary. These two models could explain the propagating velocity of an EIT wave, though the mechanism of an EIT wave is still an open question.

Surely, for a complete understanding of Moreton-wave propagation, the derivation of a realistic coronal density distribution is essential. We should search for a more reliable way to

reconstruct the actual coronal density structure, and to examine the methods developed in this work. Of course, if there are routinely space observations in Hα with high temporal cadence and resolution, we will learn about the propagating of Moreton waves more clearly.

The authors acknowledge an anonymous referee whose comments were very helpful for finishing the paper. The authors thank especially Madam M. Katota, Dr. S. Morita, Dr. E. Asano, and all other members of the Kwasan and Hida observatories for useful comments. The discussion with P. F. Chen is very appreciated. We are also grateful to all members of the SOHO EIT and MDI teams for providing the wonderful data. SOHO is a project of international cooperation between ESA and NASA. This work is supported by the Young Researcher Grant of National Astronomical Observatories, Chinese Academy of Sciences (118900KX3), the National Natural Science Foundations of China (40890161, 40974112, and 11025315), the Chinese Academy of Sciences Project KJCX2-YW-T04, and the National Basic Research Program of China (2011CB811403) and Y07024A900.

References

Aschwanden, M. J., & Acton, L. W. 2001, ApJ, 550, 475
Athay, R. G., & Moreton, G. E. 1961, ApJ, 133, 935
Benevolenskaya, E. E., Kosovichev, A. G., & Scherrer, P. H. 2001, ApJ, 554, L107
Chen, P. F. 2009, ApJ, 698, L112
Chen, P. F., Fang, C., & Shibata, K. 2005, ApJ, 622, 1202
Chen, P. F., Wu, S. T., Shibata, K., & Fang, C. 2002, ApJ, 572, L99
Chertok, I. M., & Grechnev, V. V. 2003, Astron. Rep., 47, 934
Delaboudinière, J.-P., et al. 1995, Sol. Phys., 162, 291
Delannée, C. 2000, ApJ, 545, 512
Delannée, C., & Aulanier, G. 1999, Sol. Phys., 190, 107
Eto, S., et al. 2002, PASJ, 54, 481
Gilbert, H. R., Holzer, T. E., Thompson, B. J., & Burkepile, J. T. 2004, ApJ, 607, 540
Kai, K. 1969, Sol. Phys., 10, 460
Khan, J. I., & Aurass, H. 2002, A&A, 383, 1018
Klassen, A., Aurass, H., Mann, G., & Thompson, B. J. 2000, A&AS, 141, 357
Kurokawa, H., Ishiura, K., Kimura, G., Nakai, Y., Kitai, R., Funakoshi, Y., & Shinkawa, T. 1995, J. Geomag. Geoelectr., 47, 1043
Linke, J., Ioshpa, B. A., & Selivanov, V. L. 1990, Astron. Nachr., 311, 309
Mann, G., Klassen, A., Aurass, H., & Classen, H.-T. 2003, A&A, 400, 329
Moreton, G. E. 1960, AJ, 65, 494
Moreton, G. E. 1968, Sol. Phys., 4, 30
Moreton, G. E., & Ramsey, H. E. 1960, PASP, 72, 357
Moses, D., et al. 1997, Sol. Phys., 175, 571
Nakajima, H., et al. 1994, Proc. IEEE, 82, 705
Narukage, N., Hudson, H. S., Morimoto, T., Akiyama, S., Kitai, R., Kurokawa, H., & Shibata, K. 2002, ApJ, 572, L109
Narukage, N., Ishii, T. T., Nagata, S., UeNo, S., Kitai, R., Kurokawa, H., Akioka, M., & Shibata, K. 2008, ApJ, 684, L45
Narukage, N., Morimoto, T., Kodate, M., Kitai, R., Kurokawa, H., & Shibata, K. 2004, PASJ, 56, L5
Ogawara, Y., Takano, T., Kato, T., Kosugi, T., Tsuneta, S., Watanabe, T., Kondo, I., & Uchida, Y. 1991, Sol. Phys., 136, 1
Priest, E. R. 1982, Solar Magneto-Hydrodynamics (Dordrecht: Reidel)
Priest, E. R., & Démoulin, P. 1995, JGR, 100, 23443
Scherrer, P. H., et al. 1995, Sol. Phys., 162, 129
Sheeley, N. R., Jr., Warren, H. P., & Wang, Y.-M. 2004, ApJ, 616, 1224
Smith, S. F., & Harvey, K. L. 1971, in Physics of the Solar Corona, ed. C. J. Macris (Dordrecht: Reidel), 156
Steinolfson, R. S., Wu, S. T., Dryer, M., & Tanberg-Hanssen, E. 1978, ApJ, 225, 259
Thompson, B. J., et al. 1999, ApJ, 517, L151
Thompson, B. J., Plunkett, S. P., Gurman, J. B., Newmark, J. S., St. Cyr, O. C., Michels, D. J., & Delaboudinière, J.-P. 1998, Geophys. Res. Lett., 25, 2461
Tripathi, D., & Raouafi, N.-E. 2007, A&A, 473, 951
Tsuneta, S. 1996, ApJ, 456, 63
Tsuneta, S., et al. 1991, Sol. Phys., 136, 37
Uchida, Y. 1968, Sol. Phys., 4, 30
Uchida, Y., Altschuler, M. D., & Newkirk, G., Jr. 1997, Sol. Phys., 28, 495
UeNo, S., Nagata, S., Kitai, R., Kurokawa, H., & Ichimoto, K. 2004, Proc. SPIE, 5492, 958
Vršnak, B., Magdalenić, J., Aurass, H., & Mann, G. 2002a, A&A, 396, 673
Vršnak, B., Warmuth, A., Brajša, R., & Hanslmeier, A. 2002b, A&A, 394, 299
Wang, H., Shen, C., & Lin, J. 2009, ApJ, 700, 1716
Wang, H., & Wang, J. 1996, A&A, 313, 285
Wang, J. X., Zhou, G. P., Wen, Y. Y., Zhang, Y. Z., Wang, H. N., Deng, Y. Y., Zhang, J., & Harra, L. K. 2006, CJAA, 6, 247
Wang, T. J., Yan, Y., Wang, J., Kurokawa, H., & Shibata, K. 2002, ApJ, 572, 580
Wang, Y.-M. 2000, ApJ, 543, L89
Warmuth, A., Vršnak, B., Aurass, H., & Hanslmeier, A. 2001, ApJ, 560, L105
Warmuth, A., Vršnak, B., Aurass, H., & Hanslmeier, A. 2002, in Proc. SOLSPA: 2nd Solar Cycle and Space Weather Euroconference, ed. H. Sawaya-Lacoste, SP-477 (Noordwijk: ESA), 195
Warmuth, A., Vršnak, B., & Hanslmeier, A. 2003, Hvar Obs. Bull., 27, 139
Warmuth, A., Vršnak, B., Magdalenić, J., Hanslmeier, A., & Otruba, W. 2004a, A&A, 418, 1101
Warmuth, A., Vršnak, B., Magdalenić, J., Hanslmeier, A., & Otruba, W. 2004b, A&A, 418, 1117
Wills-Davey, M. J., DeForest, C. E., & Stenflo, J. O. 2007, ApJ, 664, 556
Wu, S. T., Zheng, H., Wang, S., Thompson, B. J., Plunkett, S. P., Zhao, X. P., & Dryer, M. 2001, J. Geophys. Res., 106, 25089
Yan, Y., & Sakurai, T. 2000, Sol. Phys., 195, 89
Zhang, J., White, S. M., & Kundu, M. R. 1999, ApJ, 527, 977
Zhang, J., Zhou, G., Wang, J., & Wang, H. 2007, ApJ, 655, L113
Zhang, Y., Wang, J., Attrill, G. D. R., Harra, L. K., Yang, Z., & He, X. 2007, Sol. Phys., 241, 329
Zhao, X. P., Hoeksema, J. T., & Scherrer, P. H. 1997, in Proc. 5th SOHO Workshop: The Corona and Solar Wind Near Minimum Activity, ed. A. Wilson, SP-404 (Noordwijk: ESA), 751
Zhukov, A. N., & Auchère, F. 2004, A&A, 427, 705